JCTC Journal of Chemical Theory and Computation

Systematic Coarse-Graining of a Polymer Blend: Polyisoprene and Polystyrene

Qi Sun and Roland Faller*

Department of Chemical Engineering and Materials Science, University of California—Davis, Davis, California 95616

Received February 16, 2006

Abstract: The Iterative Boltzmann Inversion technique (also known as the Inverse Boltzmann Method) is generalized to polymer blends. We systematically optimize a mesoscale model against the structure of the blend. A polyisoprene−polystyrene blend is used as an example. Atomistic simulations of a blend of short chains in the miscible regime under melt conditions are taken as a starting point. We optimize the mesoscale model and study the onset of phase separation with increasing chain length. The mesoscale model phase separates at a chain length of 15 monomers where it was optimized, whereas the atomistic model shows only a preference of chains to aggregate to neighborhoods of like chains. We discuss the differences of the optimization between a blend and a homopolymer system in detail.

I. Introduction

Multiscale modeling of homopolymers has been successfully applied using a variety of techniques.[1−6] One particularly successful technique is known as the Inverse Boltzmann Method or Iterative Boltzmann Inversion (IBI).[7−11] Reliable models for a number of polymers have been developed using this technique, and the corresponding static and dynamic behaviors have been investigated. For example, recently, we could show that we can semiquantitatively estimate the entanglement length of polystyrene using this technique.[11]

The state of the art in the systematic modeling of polymer blends is much less satisfactory. The main obstacle is the lack of so-called "mixing rules". Unlike in the case of atomistic simulations, the equivalence of, say, Lorentz−Berthelot rules cannot be applied in structurally coarse-grained blends. It becomes immediately clear that the unlike interactions between different constituents have to be treated completely independently from the like interactions because the nature of these interaction stems from the interplay of the energetics and the local chain packing. Especially, the latter cannot be predicted for a mixture even if the behaviors of the pure components are known. Moreover, the resulting potentials may be concentration- and temperature-dependent because any systematically optimized model depends on the thermodynamic state against which it was optimized. We recently showed for a polystyrene model that the reliable temperature range of an optimized model may indeed be very limited.[12]

In this light, we elucidate the possibility to optimize a coarse-grained model for a blend of polyisoprene (PI) and polystyrene (PS) as a test case. Experimentally, this system is known to be miscible at short chain lengths,[13,14] and demixing is observed at longer chain lengths.[14] We are embarking on this specific system because there are systematically coarse-grained models of the pure components available.[8,10] This system has, for short chain lengths, recently attained some attention due to its interplay of short and large lengths and time-scale dynamics.[13,15,16] Because atomistic simulations are not able to equilibrate the terminal relaxation even of miscible short-chain systems, a mesoscale approach will be helpful for understanding such dynamic questions as well.

This paper is organized as follows: We first briefly describe the atomistic simulations on which the mesoscale modeling is based. Then, we explain in detail how the mesoscale modeling is performed with a focus on optimizing interactions between different polymers. The large-scale simulations are analyzed, and we finish with conclusions.

II. Simulation Investigations

A. Atomistic Simulations of a *cis*-PI and PS Melt Mixture. Polymer blends of *cis*-PI and atactic PS are investigated

* Corresponding author fax: 530-752-1031; e-mail: rfaller@ucdavis.edu.

10.1021/ct600065v CCC: $33.50
Published on Web 04/08/2006

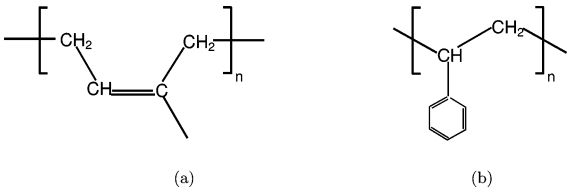

Figure 1. (a) PI monomer and (b) PS monomer.

in atomistic detail to obtain the input parameters for the mesoscale model. Figure 1 shows the structures of the atomistic monomers of *cis*-PI and PS. We choose to simulate chains of a length of 15 monomers in atomistic detail. These are clearly oligomers; however, it has been shown that for such lengths the chains are not completely dominated by end effects[17] such that a reliable structure optimization should be possible. Longer chains would definitely not equilibrate in reasonable computer time for an atomistic model. Moreover, experiments suggest that chains of this length should be miscible, but an effect of the demixing at longer chain lengths is expected.[13] Our atomistic simulations are performed at a variety of concentrations where the number of PS or PI chains varies between 24 and 72 for the two constituents. The subsequent optimization is based on a system with 24 PS and 36 PI chains, corresponding to a blend of 50 wt %. For the force field of PS, we use the Lennard-Jones parameters of Jorgensen and Severance.[18] The bending potential from all of the angles, the torsion potentials for all of the backbone and phenyl ring carbons, and the improper potentials which keep the phenyl groups planar are taken from refs 19 and 20. All 1−4 nonbonded interactions of PS atoms are excluded. The bond lengths and angles for the atomistic PI simulation and the potentials associated with the bonds, angles, and improper dihedrals are adapted from previous simulations.[21,22] Atoms connected by any bonding potentials do not interact by the Lennard-Jones potential. Further nonbonded interactions are excluded following the rules addressed in ref 23. All of the bond lengths are constrained using the LINCS algorithm.[24] The simulations are conducted using molecular dynamics (MD) at 450 K and a pressure of 101.3 kPa for 20 ns. Constant temperature and pressure are ensured using the weak coupling method[25] with time constants of 0.2 ps for temperature and 1.0 ps for pressure. A compressibility of 1.12×10^{-6} kPa^{-1} is applied to the three Cartesian directions independently. Simulations are performed using the GROMACS software[26] with a time step of 2 fs and a cutoff for nonbonded interactions at 1.2 nm. Configurations are saved every 2000 steps. A detailed analysis of the atomistic simulations in view of the local dynamics will appear elsewhere.[27]

B. Mapping from Atomistic Scale to Mesoscale. Mapping simulation models derives the input parameters of a mesoscale model from an atomistic simulation. The following tasks need to be solved during the mapping. First, we need to determine the location of superatom centers along the chains. A superatom is the unit containing a number of atomistic atoms which are grouped together and are represented by a single interaction center on the larger scale. The principle of selecting the superatom center is that the superbonds between superatoms can be represented with a single harmonic potential.[5,6] Moreover, we want the potentials for superangles and -torsions to be simple or, ideally, to vanish completely. For PS, we tried several possible positions on the backbone or the side-group carbons. We calculated the bond distributions along the polymer chains for all of them. Only the superatom locations which result in narrow Gaussian distributions for the bond lengths fulfill the above requirement. The height-to-width ratio of the bond distributions defines the harmonic bond strength. The distance corresponding to the maximum of the distribution defines the superbond length. The superatom centers of PS were finally chosen on the backbone carbons connecting to the phenyl rings.[10] The superatom centers of PI are placed on the centers of the single bonds connecting two neighboring atomistic monomers.[8] The angle distribution and angle potentials were determined from the atomistic simulation as well. Three consecutive superatom centers form a superangle. All angle distributions were normalized and averaged, excluding the three superatoms closest to either chain end. The resulting distributions are divided by the sine of the corresponding angles as Jacobian and normalized.[5,6] A running average of length 3 is additionally applied. The angle distributions are resolved to an accuracy of 1°. The angle forces are calculated as the logarithmic difference between two consecutive angle distributions. Again, a running average of 3 is applied. A torsion potential is not needed for the polymers under study.

In MD, generally, interactions between particles are chosen to be analytic functions with a few adjustable parameters. Our work derives a numerical potential for the nonbonded interaction which is dependent on the radial distribution functions (RDFs). These distribution functions are a good choice to describe the structure of polymers, keeping the identity of the polymer structure. We use IBI[9] to reproduce the structure by means of RDFs. Because this technique has been discussed in detail in a number of publications,[8−10] we focus only on the modifications due to the blend. The generalization to binary blends requires three potentials from the corresponding distribution functions: PI−PI, PS−PS, and PI−PS. We obviously first need two sets of superbond length and superangle distributions, together with bending potentials and angle potentials, which are directly transferred from our earlier work.[8,10]

The IBI method obtains a numerical force field; that is, the potential values are specified by a tabulation on a grid of equidistant distances or angles. For the nonbonded interaction, we use a grid resolution of 0.01 times the repulsive core of the interaction as measured at its zero passage (i.e., 0.01σ in the case of a Lennard-Jones potential). The whole procedure relies on serially executed iterations.

In dense systems, individual distributions depend on the full set of potentials through higher-order correlation. For technical reasons, one can keep the majority of potentials constant while iterating a particular one; the rest has to be readjusted afterward, one by one. For practical purposes, it is effective to start with those potentials that are least affected by changes in the others. This is not a trivial a priori knowledge but typically found during the initial steps of the

optimization. In our case, we found that the PI−PI and PS−PS pairs are relatively independent of each other compared to the degree to which they interdepend on the PI−PS potential. This is not too surprising because we expect a tendency to demix, and therefore, the PI−PI potential should not change the PS−PS structure and vice versa. Basically, the like pairs can be optimized in parallel. Especially, the PI−PI structure is quasi independent of PS−PS or, to a lesser extent, PI−PS potentials. The PS−PS structure is influenced more strongly by the PI−PS potential. Examples of RDFs during the optimization are shown in Figure 2. All optimization focuses on the local structure, that is, up to 1 nm for PI−PI and 1.8 nm for both PS−PS and PI−PS. It has been shown in our earlier work that the PI and PS structures have different sensitivities to the neighborhood between 1 and 1.8 nm. After each iteration, the radial distribution function $g(r)$ was checked carefully to make sure all of the target structures were present, as well as if there were any nonphysical structures involved. These may stem from, for example, cutoffs. The potential at the cutoffs should be set to 0 to ensure energy conservation. We adjust the potential to 0 by shifting all values, keeping the shape fixed. Our optimization obtains the correct structure by removing unwanted features and optimizing to the desirable structure as close as possible. First, we focus on removing undesired features. Small humps or spurious corners, as, for example, seen in 15th iteration of the PS−PS RDF (cf. 4), are likely associated with humps or spurious corners in the potential. Smoothing gets rid of the above problems. When the general features are reproduced and only smaller changes are needed, adjusting the initial slope of the potential is a good starting point. This means we do not optimize all length scales of the potential at one time but focus on smaller windows, starting from shorter length scales.[10] During the optimization of the PS−PS pair, we ran into a problem that the first peak in the $g(r)$ around $r \approx 1.2$ nm was clearly wider than the target peak. We found in this case that it was more efficient to change the slope of the potential manually instead of continually optimizing consistently according to the IBI

$$\Delta V(r) = -k_B T \ln\left[\frac{g(r)}{g_{\text{target}}(r)}\right] \quad (1)$$

where ΔV is the correction potential from a direct Boltzmann inversion of the difference between the RDF of the corresponding iteration $g(r)$ and the atomistic target g_{target}.

The speed of convergence is influenced by the order in which one optimizes the various potentials. We started the optimization with the PI−PI potential, followed by the optimization of PS−PS, and the interaction of PI−PS is dealt with during the late stages of the PS−PS iteration.

C. Adapting the Pressure. We started with a purely structural optimization of the PI−PS system. Our best potential, however, yields a positive pressure of $P^* = 1.92$ in dimensionless units defined equivalently to the standard Lennard-Jones units. $P^* = 1.92$ corresponds to $P = 1.192 \times 10^7$ Pa as calculated by $P = P^*\epsilon/\sigma^3$.[28] This does not reflect the ambient conditions of the parent atomistic system. This

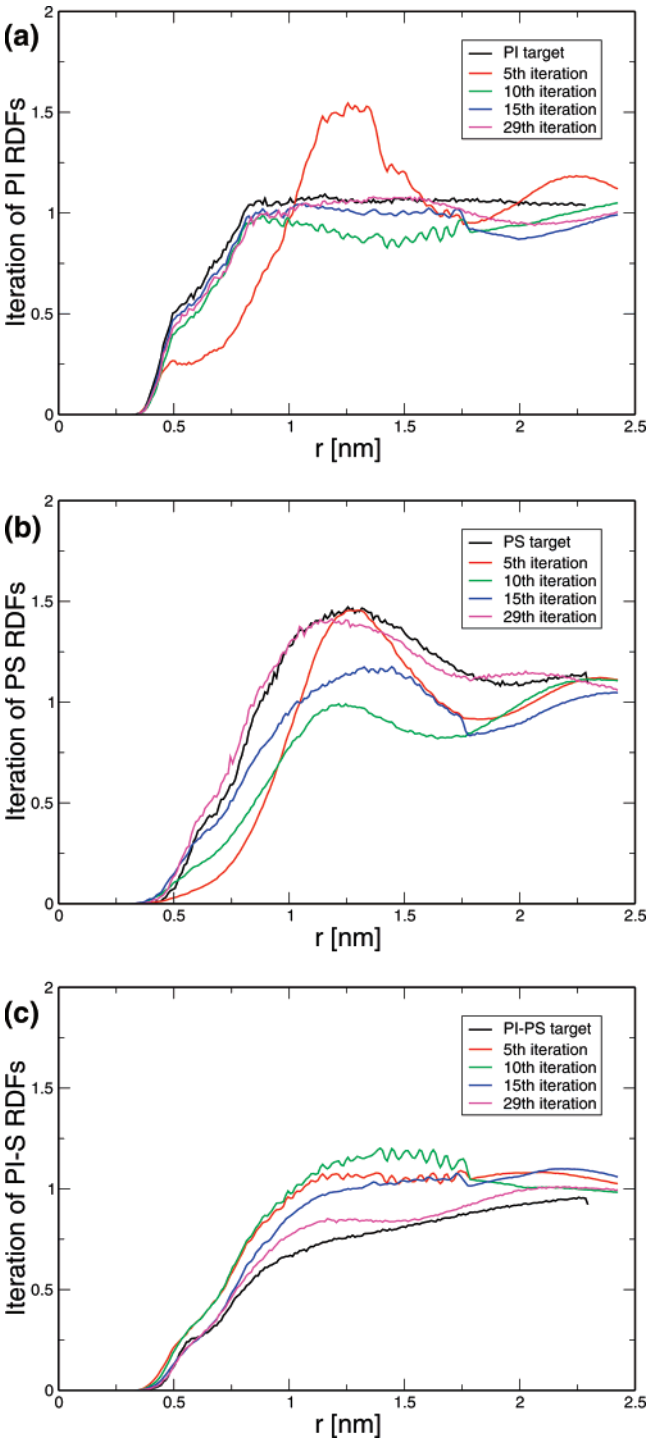

Figure 2. (a) Iteration of PI RDFs, (b) iteration of PS RDFs, and (c) iteration of PI−PS RDFs.

is a consequence of the simulation being run at a constant volume and thermodynamic properties not being used in the optimization. As a proof of concept that pressure correction is possible in a blend, we tried to postoptimize the mesoscopic system without lowering the quality of RDFs. The potential of a system without charges is always attractive at long ranges because of the dispersion interactions, and a corresponding pressure correction technique has been suggested.[7] Consequently, we choose an attractive linear tail function as a weak perturbation to the three potentials previously optimized without pressure correction:

$$\Delta V_{\mathrm{lim}}(r) = A_i\left(1 - \frac{r}{r_{\mathrm{cutoff}}}\right) \qquad i = 1, ..., 3 \qquad (2)$$

with A_i taking small values ranging from 0 to $-0.1\ k_BT$. The A_i values are different for the three interactions. The corrected potentials were taken as initial guesses in a reoptimization of the potentials against the structure using IBI. After that, the pressure was re-evaluated. Combined with optimum results of the RDFs, an improvement to $P^* \approx 1.3$ is obtained. This condition was reached after 10 iteration cycles. The pressure correction focuses in the potential region beyond $r > 1$ nm, which is not very important for the structural fit. It shifts the whole potentials downward, thus providing for the previously missing long-range attraction. However, we did not find significant differences in the overall structure of the system, and the fundamental results below are the same with and without pressure correction.

The optimization took about 35 runs to obtain the resulting RDFs. Each iteration runs for 3000 τ, after which the system with a new set of potentials could attain an equilibrium. We confirmed that, between 1000 and 3000 τ, the RDFs did not change.

D. Mesoscale Simulation. The PI−PS blends are investigated in the *NVT* ensemble for the mesoscale simulations. The reduced temperature ($T^* = k_BT/\epsilon$) is set to 1, where ϵ is the interaction energy between pairs of atoms. σ^* is set to 1 nm. The density is 6.4175 monomers/σ^3 according to the atomistic parent simulation. The temperature is maintained by a Langevin thermostat with a friction constant $\Gamma = 1.0\ \tau^{-1}$, where $\tau = \sqrt{\sigma^2 m/\epsilon}$.[28] We use an orthorhombic box under periodic boundary conditions. The initial condition is directly transferred from an atomistic simulation. The equation of motion is integrated with a time step $\Delta t = 0.005\ \tau$, which is the smaller of the time steps used in the simulations of pure PI and PS.[8,10,11] Trajectories are stored every 2000 steps. The superbond length of PI is 0.2345 nm with a strength of 0.0015 k_BT, while that of PS is 0.2545 nm with a strength of 0.03 k_BT. The cutoff for the nonbonded interactions is 1.910σ, which is the bigger of the PI and PS cutoffs of the pure systems. The numerically optimized potential from the system of the 36 PI and 24 PS chains of length 15 is applied to all systems. The details of the investigated systems are listed in Table 1.

III. Results and Discussion

A. Structure. To test the transferability of applying bond or angle structures to polymer blends, the bond length and bond angle distributions and potentials of PS from both 48 PS chains systems and the blend of 36 chains of PI and 24 chains of PS were compared and plotted in Figure 3. The bond distributions clearly show the same pattern in the pure PS and in a polymer blend with 36 chains of PI; however, the PS−PS−PS bond angle force shows some discrepancies. These stem from the effect of local packing because a number of the PS−PS intermolecular interactions are replaced by PS−PI contacts. Here, we kept the intramolecular potentials of the pure systems for transferability purposes.

During all of our simulations for optimization and analysis, we ensured that the chains diffuse at least $2\langle R_g^2\rangle$ such that the configurations are fully relaxed. We then checked each system by monitoring the radius of gyration (R_g) and $\langle R_g^2\rangle$ to make sure that the systems attained equilibration. Our results for the persistence lengths l_p given by $l_p \approx 0.65$ nm are independent of the chain length for $10 \leq N \leq 80$.

The RDFs of the atomistic and optimized mesoscale simulations are plotted in Figure 4. These are both shown for 15 monomers. This is the best potential after 35 iterations. The optimization result is judged by the sum of the squared difference between the target and the optimized $g(r)$. Compared to a pure polymer melt, the iteration of blends is technically more demanding in that mapping takes into account the effects of three sets of potentials. Therefore, the quality of the optimized RDFs is somewhat weaker than that for pure systems. Because the PI−PI or PS−PS pair interacts with the inter-PI−PS pair, iterating each pair induces deviations in other pairs. Examples of radial distribution functions during the iteration are plotted in Figure 2. Our work provides the first application in the system of a binary blend with reasonable consistency.

B. Phase Separation. Using our mesoscale model, we can embark now on a study of the phase behavior of the blend focusing on the following questions: What morphologies do we obtain, and how do they depend on concentration? How does an initially randomly distributed configuration evolve into a phase-separated system? By increasing chain length, where is the crossover between miscibility and phase separation? The visualization of PI−PS blends with a fixed mass concentration ratio of 1:1 shows the evolution of phase separation in Figure 5. In the initial configuration of the system with 36 PI and 24 PS chains, both of length 60, the components are well-mixed, as shown in Figure 5a. Increasing times of 300, 600, 1000, 2000, and 20 000 τ show the evolution of phase separation. Starting from the beginning, the PS chains (dark red spheres) show a tendency toward aggregation. At 600 τ, the aggregated PS chains take on a cylindrical shape with a few PS chains in the PI majority phase. The PS region is only separated by several PI chains in the middle (Figure 5d). The final snapshot at 20 000 τ shows the equilibrium. We now have a clearly lamellar pattern as expected for an equiconcentrated mixture.

Besides the lamellar morphology shown for the 36 PI 60-mer−24 PS 60-mer system, we investigate the phase separation dependent on the PI chain length with a fixed PI/PS weight ratio (50:50). Figure 6 shows lamellar shapes for the 72 PI 10-mer−48 PS 10-mer and 36 PI 30-mer−24 PS 30-mer systems. Cylindrical shapes are observed in Figure 7 for 36 PI chains of length 45 with the 24 PS 30-mer and for the 36 PI 60-mer−4 PS 30-mer system. In the systems of 72 PI 10-mer−48 PS 10-mer, 36 PI 30-mer−24 PS 30-mer, and the above 36 PI 60-mer−48 PS 60-mer, the weight ratio of PI to PS monomer weight concentration is kept fixed at 50:50. We conclude that at balanced concentrations the morphology of PI−PS blends is lamellar. As the concentration of PI to PS monomers changes to 60:40, as in the case of 36 PI 45-mer−24 PS 30-mer, or even higher to 66:34, as in the case of 36 PI 60-mer−24 PS 30-mer, the systems prefer a cylindrical morphology, as shown in Figure

Table 1. Characterizations of PS and PI Chains at Various Concentrations

		PI				PS			
N_c	box size	R_g	R_g^2	l_p (bond)	l_p (nm)	R_g	R_g^2	l_p (bond)	l_p (nm)
72PI7/48PS7	5.0774	0.3448	0.1206	1.5921	0.3733	0.3906	0.1539	1.9341	0.4922
72PI10/48PS10	5.7184	0.4795	0.2330	2.2002	0.5159	0.5272	0.2804	2.3639	0.6016
72PI14/48PS15	6.4574	0.6229	0.3940	2.5806	0.6052	0.7153	0.5188	2.6351	0.6706
72PI15/48PS15	6.5459	0.6234	0.3936	2.6317	0.6171	0.7139	0.5152	2.8987	0.7377
36PI30/24PS30	6.5459	1.0789	1.1930	2.7503	0.6449	1.1519	1.3598	2.6861	0.6836
36PI30/24PS45	6.9560	1.0801	1.1964	2.6889	0.6305	1.3821	1.9759	2.4283	0.6180
36PI30/24PS60	7.3228	1.0808	1.1944	2.6590	0.6235	1.7505	3.1953	2.6070	0.6635
36PI30/24PS80	7.7610	1.0777	1.1884	2.7108	0.6357	2.0348	4.2990	2.5715	0.6544
36PI45/24PS30	7.1441	1.4239	2.0921	3.0102	0.7059	1.1473	1.3491	2.6334	0.6702
36PI60/24PS30	7.6561	1.6746	2.9071	2.9246	0.6858	1.1192	1.2888	2.6019	0.6622
36PI80/24PS30	8.2473	2.0446	4.3507	2.8551	0.6695	1.0716	1.1775	2.7668	0.7041
36PI60/24PS60	8.2473	1.6873	2.8422	2.7252	0.6391	1.7793	3.2170	2.4545	0.6247
36PI80/24PS80	9.0773	1.9113	3.9538	2.9011	0.6803	1.9321	4.0789	2.6153	0.6656

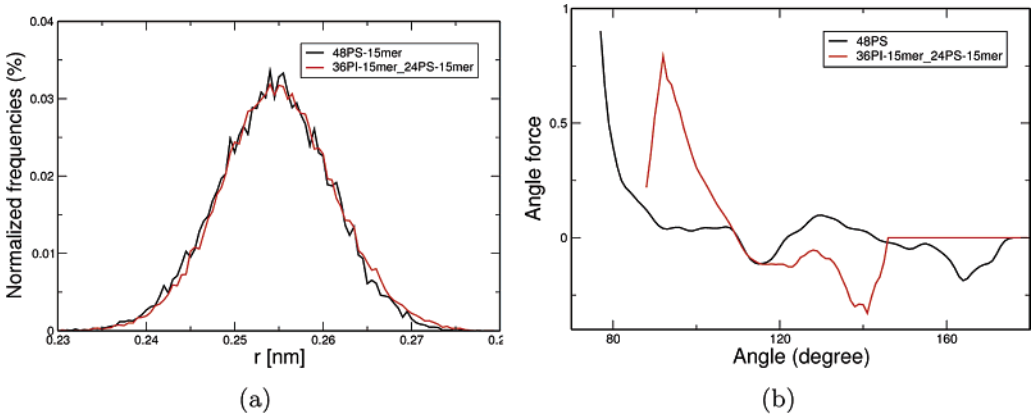

Figure 3. Comparison of the intramolecular potentials in the homopolymer melt and the 50 wt % blend. (a) PS bond distribution and (b) PS angle force.

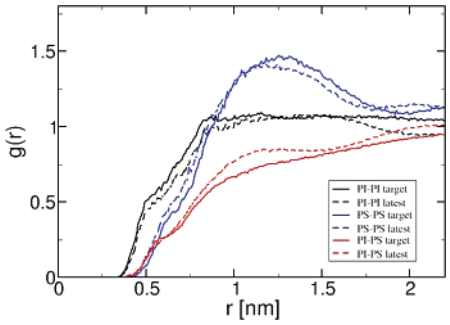

Figure 4. RDFs of the PI−PS mixture melt.

7. The radius of the PS cylinder decreases as the PI chain length increases from 45 to 60.

Figure 8 shows a well-mixed configuration of the 72 PI 7-mer−48 PS 7-mer system at 10 000 τ. Compared to chains of lengths 10, 30 (in Figure 6), and 60 (in Figure 5), the phase separation starts above 7 monomers. Note that, both in atomistic simulations and in experiments, the system is still mixed at 15 monomers, whereas we observe a phase separation tendency. However, the atomistic simulations are only 20 ns long, and the radial distribution functions for the 15-mers are by construction consistent between the atomistic and mesoscale systems. This study shows again that one structural characteristic alone leads typically to good potentials but some discrepancies between the atomistic and mesoscale models remain and the finite-size of the system may play a role.

C. RDFs of Superatoms. Intermolecular pair distributions of PI−PI and PS−PS monomers are calculated and shown in Figure 9. Figure 9a illustrates that, at constant conditions of 36 PI chains of chain length 30, the inter-PI−PI $g(r)$ increases with the PS chain length, which means the PI monomers increasingly prefer a PI neighborhood. Phase separation can explain this observation, as suggested by previous results. Figure 9b shows that the correlation hole dominates as the number of inter-PI−PI pairs decreases with the increase of the PI chain length at a constant PS chain length. A correlation hole means that with increasing chain length the chain itself provides a non-negligible number of neighboring monomers and, by this, suppresses the interchain RDF.[30,31] The interchain radial distribution functions of like monomers here probe for long chains, essentially a homopolymer system, because of the phase behavior. Figure 9d illustrates that at the same condition of 36 PI chains of the 30-mer, as in Figure 9a, the PS−PS pairs decrease with the increase of the PS chain length, opposite of the increasing trend of the PI−PI pairs. Figure 9c demonstrates that the number of PS−PS pairs increases generally with the increase of the PI chain length in the mixture with 24 PS 30-mers,

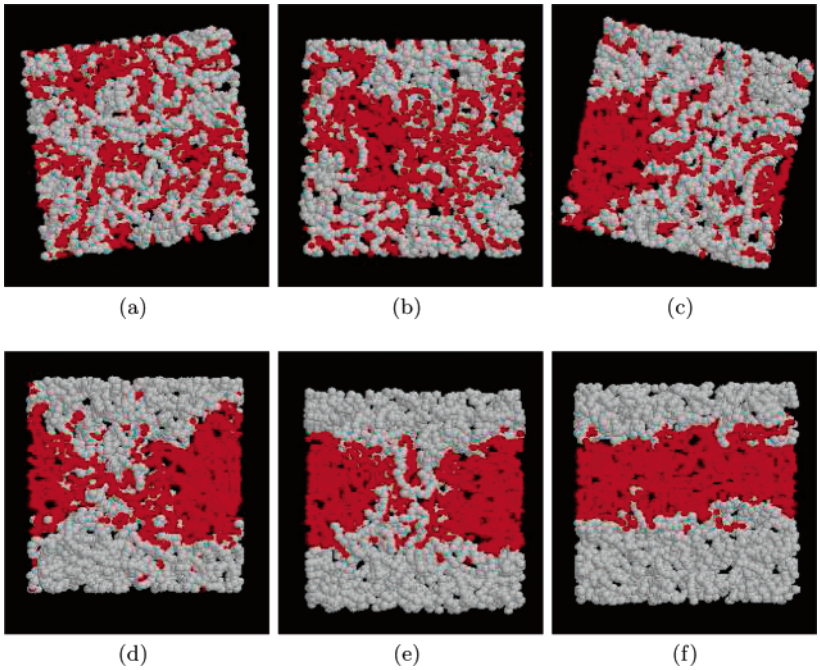

Figure 5. Snapshots of 36 PI 60-mer−24 PS 60-mer systems at various times: (a) starting configuration (time 0), (b) $t^* = 300\ \tau$, (c) $t^* = 600\ \tau$, (d) $t^* = 1000\ \tau$, (e) $t^* = 2000\ \tau$, and (f) $t^* = 20\ 000\ \tau$. The light spheres represent the polyisoprene superatoms, and dark red ones are polystyrene. The program RASMOL[29] was used for the visualization.

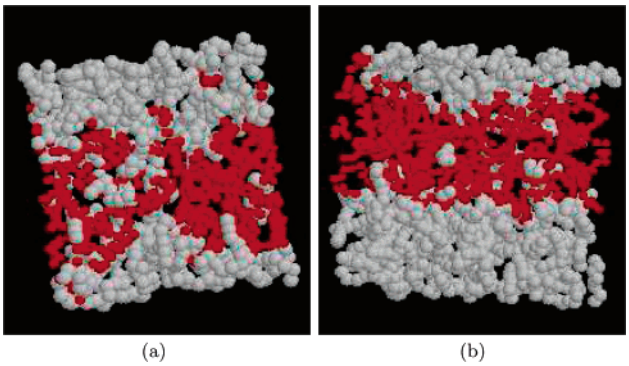

Figure 6. Snapshots of polymer mixture systems at various chain lengths: (a) 72 PI 10-mer−48 PS 10-mer at a unit time of 10 000 τ and (b) 36 PI 30-mer−24 PS 30-mer at a unit time of 10 000 τ.

except for the 80-mer case, which we again attribute to a correlation hole effect. Overall, the trends show that the number of pairs of the fixed chain length and the number of chain polymers increase with the chain length of the opposite component, while those of the varying polymers themselves decrease.

To test the dependence of phase separation on the chain length, we increase the chain length of both polymers from 10 to 30, 60, and 80 monomers. The concentration of PI and PS is kept fixed at 50:50 by weight. Pair distributions of inter-PI−PI, inter-PS−PS, and PI−PS are calculated to obtain a general picture of distribution. For comparison, the atomistic parent simulations at length 15 are shown as well. All intrapairs are excluded. Figure 10 shows that the interchain radial distribution function of PI−PI does not change as much as that of PS−PS or PI−PS. At the region of distance $r < 1.0$ nm, the $g(r)$ values of PI−PI pairs decrease as the chain length increases from 10 to 30, 60,

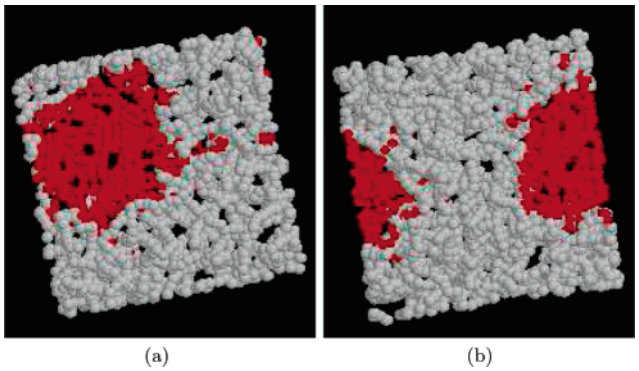

Figure 7. Snapshots of polymer systems (a) 36 PI 45−24 PS 30 at a unit time of 10 000 τ and (b) 36 PI 60−24 PS 30 at a unit time of 10 000 τ.

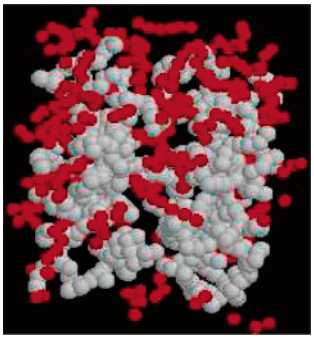

Figure 8. 72 PI 7-mer−48 PS 7-mer at a unit time of 10 000 τ.

and 80 monomers. The reason is the increasing radius of gyration. The PI−PI interactions show that PI monomers prefer their own neighborhood from $r > 1.0$ nm up to 3.0 nm. The PS−PS RDF (Figure 10b) shows a consistent trend of moving closer together as the chain length of PS increases.

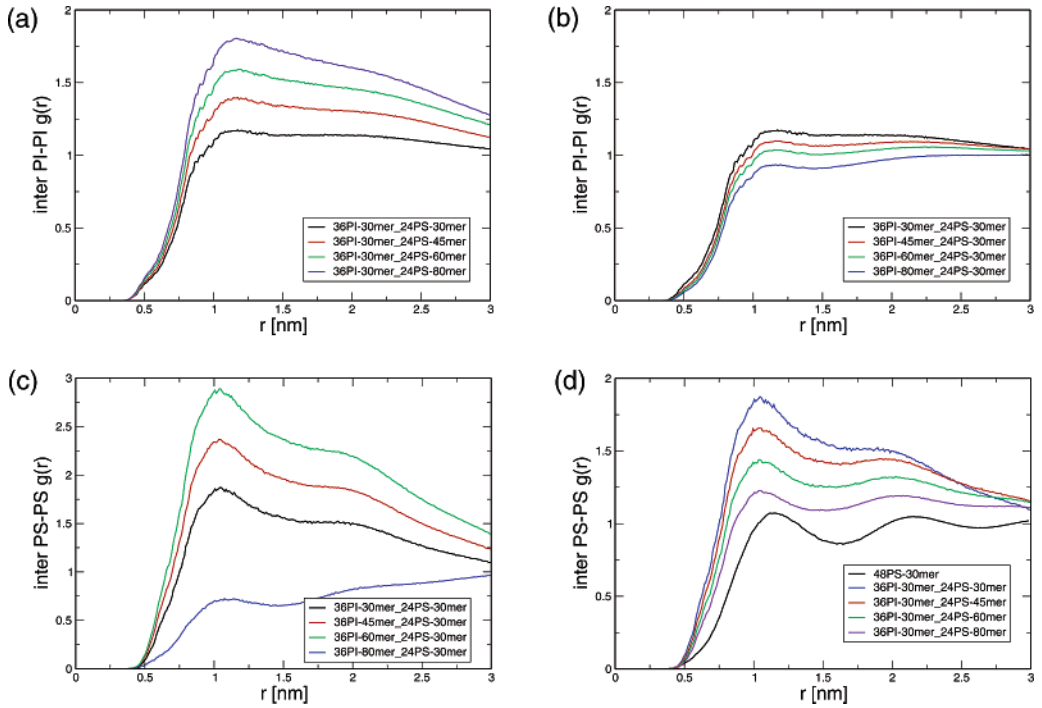

Figure 9. (a) Inter-PI−PI $g(r)$ at fixed 36 PI 30-mer, (b) inter-PI−PI $g(r)$ at fixed 24 PS 30-mer, (c) inter-PS−PS $g(r)$ at fixed 24 PS 30-mer, and (d) inter-PS−PS $g(r)$ at fixed 36 PI 30-mer.

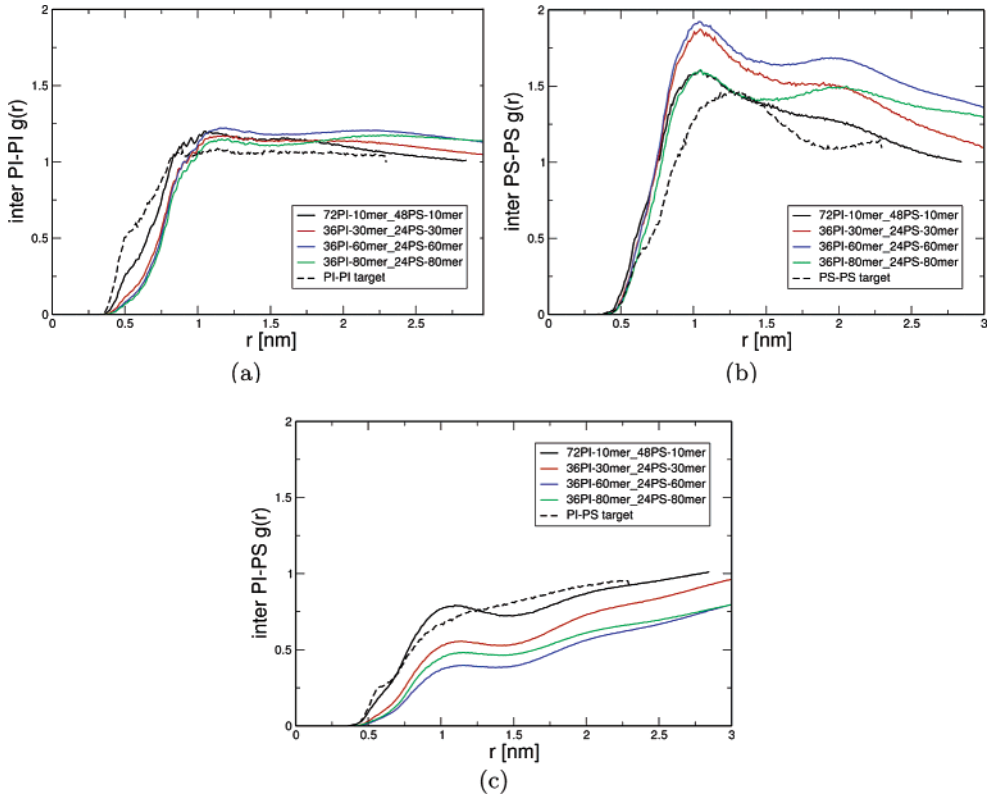

Figure 10. (a) Inter-PI−PI $g(r)$ at fixed PI/PS ratio of 1:1, (b) inter-PS−PS $g(r)$, and (c) inter-PI−PS $g(r)$.

Consider that the phase morphology does not change except for a chain length of 80; increasing the chain length leads to fewer contacts of PI−PS and correspondingly more PS−PS interactions. Moreover, we expect the phase separation to become stronger, that is, the PS region to have an even higher PS concentration at long chain lengths. PI−PS (in Figure 10c) pairs have a peak and a valley at short distances $r <$ 1.5 nm and increase gradually to a value of 1.0 near 3.0 nm. However, the number of PI−PS pairs decreases with the increase of the chain length, indicating that the PI and PS chains are more separated from each other. At the chain length of 80 monomers, all $g(r)$ functions show a different trend; PI−PS pairs increase instead of decrease. This can be explained by a cylindrical instead of a lamellar morphol-

ogy. Take the three RDFs as a whole; the PS−PS structures have two peaks throughout the entire chain length. The peak positions are at 1.5∼2.0 nm, which are at greater distances than those of PI−PI. It indicates that PS−PS has a stronger tendency to its own neighborhood. The PI−PS RDFs show consistently unfavorable interactions.

IV. Conclusion

We have shown here for the first time that the Iterative Boltzmann Inversion can be applied to a binary blend of polymers. The resulting potentials lead to results in qualitative agreement with expected experimental behavior. We are able to equilibrate systems which are phase-separating and observe the dynamics of the phase separation for the first time by a systematically coarse-grained blend.

It is worth stressing that we expect that the resulting potentials are dependent on concentration and temperature, and further studies to elucidate the phase diagram are under way. They are, however, stable under a change of chain length.

It is furthermore worth mentioning that there is no clear and obvious order in which of the optimizations should be conducted. The various potentials are strongly interdependent, and we observed that changing the order of optimization can have a serious influence on the efficiency of the convergence.

The phase separation sets in at around seven monomers, which is shorter than in experiments and also shorter than in the parent atomistic simulations. This again shows that we cannot expect all observables to be in agreement when we did not specifically optimize against them. It additionally shows that we have to develop such polymer blend models at short chain lengths in order to increase the number of unlike contacts for optimization. For a close to equimolar concentration, we find predominantly lamellar morphologies as expected. Other morphologies can be reproduced as well.

Acknowledgment. Financial support from the U.S. Department of Energy, Office of Advanced Scientific Computing, under grant DE-FG02-03ER25568 is gratefully acknowledged.

References

(1) Tschöp, W.; Kremer, K.; Batoulis, J.; Bürger, T.; Hahn, O. Simulation of Polymer Melts. I. Coarsegraining Procedure for Polycarbonates. *Acta Polym.* **1998**, *49*, 61−74.

(2) Baschnagel, J.; Binder, K.; Doruker, P.; Gusev, A. A.; Hahn, O.; Kremer, K.; Mattice, W. L.; Müller-Plathe, F.; Murat, M.; Paul, W.; Santos, S.; Suter, U. W.; Tries, V. Bridging the Gap between Atomistic and Coarse-Grained Models of Polymers: Status and Perspectives. *Adv. Polym. Sci.* **2000**, *152*, 141−156.

(3) Müller-Plathe, F. Coarse-Graining in Polymer Simulation: From the Atomistic to the Mesoscopic Scale and Back. *ChemPhysChem* **2002**, *3*, 754−769.

(4) Müller-Plathe, F. Scale-Hopping in Computer Simulations of Polymers. *Soft Mater.* **2003**, *1*, 1−31.

(5) Faller, R. Automatic Coarse Graining of Polymers. *Polymer* **2004**, *45*, 3869−3876.

(6) Faller, R. Coarse-Grain Modeling of Polymers. *Rev. Comput. Chem.* **2006**, *23*, in press.

(7) Reith, D.; Meyer, H.; Müller-Plathe, F. CG-OPT: A Software Package for Automatic Force Field Design. *Comput. Phys. Commun.* **2002**, *148*, 299−313.

(8) Faller, R.; Reith, D. Properties of Polyisoprene Model Building in the Melt and in Solution. *Macromolecules* **2003**, *36*, 5406−5414.

(9) Reith, D.; Pütz, M.; Müller-Plathe, F. Deriving Effective Mesoscale Potentials from Atomistic Simulations. *J. Comput. Chem.* **2003**, *24*, 1624−1636.

(10) Sun, Q.; Faller, R. Systematic Coarse-Graining of Atomistic Models for Simulation of Polymeric Systems. *Comput. Chem. Eng.* **2005**, *29*, 2380−2385.

(11) Sun, Q.; Faller, R. Crossover from Unentangled to Entangled Dynamics in a Systematically Coarse-Grained Polystyrene Melt. *Macromolecules* **2006**, *39*, 812−820.

(12) Ghosh, J.; Wong, B. Y.; Sun, Q.; Pon, F. R.; Faller, R. Simulations of Glasses: Multiscale Modeling and Density of States Monte Carlo Simulations. *Mol. Simul.* **2006**, in press.

(13) He, Y.; Lutz, T. R.; Ediger, M. D.; Pitsikalis, M.; Hadjichristidis, N.; von Meerwall, E. D. Miscible Polyisoprene/Polystyrene Blends: Distinct Segmental Dynamics but Homogeneous Terminal Dynamics. *Macromolecules* **2005**, *38*, 6216−6226.

(14) Koningsveld, R.; MacKnight, W. J. Liquid−Liquid-Phase Separation in Multicomponent Polymer Systems XXVII. Determination of the Pair Interaction Function for Polymer Blends. *Polym. Int.* **1997**, *44*, 356−264.

(15) He, Y.; Lutz, T. R.; Ediger, M. D. Segmental and Terminal Dynamics in Miscible Polymer Blends. *J. Chem. Phys.* **2003**, *119*, 9956−9965.

(16) Lutz, T. R.; He, Y.; Ediger, M. D.; Pitsikalis, M.; Hadjichristidis, N. Dilute Polymer Blends: Are the Segmental Dynamics of Isolated Polyisoprene Chains Slaved to the Dynamics of the Host Polymer? *Macromolecules* **2004**, *37*, 6440−6448.

(17) Faller, R. Correlation of Static and Dynamic Inhomogeneities in Polymer Mixtures: A Computer Simulation of Polyisoprene and Polystyrene. *Macromolecules* **2004**, *37*, 1095−1101.

(18) Jorgensen, W. L.; Severance, D. L. Aromatic−Aromatic Interactions: Free Energy Profiles for the Benzene Dimer in Water, Chloroform. *J. Am. Chem. Soc.* **1990**, *112*, 4768−4774.

(19) Müller-Plathe, F. Local Structure and Dynamics in Solvent-Swollen Polymers. *Macromolecules* **1996**, *29*, 4782−4791.

(20) Sun, Q.; Faller, R. Molecular Dynamics of a Polymer in Mixed Solvent: Atactic-Polystyrene in a Mixture of Cyclohexane and N,N-dimethylformamide. *J. Phys. Chem. B* **2005**, *109*, 15714−15723.

(21) Faller, R.; Schmitz, H.; Biermann, O.; Müller-Plathe, F. Automatic Parametrization of Force Field for Liquids by Simplex Optimization. *J. Comput. Chem.* **1999**, *20*, 1009−1017.

(22) Schmitz, H.; Faller, R.; Müller-Plathe, F. Molecular Mobility in Cyclic Hydrocarbons—A Simulation Study. *J. Phys. Chem. B* **1999**, *103*, 9731−9737.

(23) Faller, R.; Müller-Plathe, F.; Doxastakis, M.; Theodorou, D. Local Structure and Dynamics of *trans*-Polyisoprene Oligomers. *Macromolecules* **2001**, *34*, 1436−1448.

(24) Hess, B.; Bekker, H.; Berendsen, H. J. C.; Fraaije, J. G. E. M. LINCS: A Linear Constraint Solver for Molecular Simulations. *J. Comput. Chem.* **1997**, *18*, 1463−1472.

(25) Berendsen, H. J. C.; Postma, J. P. M.; Gunsteren, V.; Haak, J. R. Molecular Dynamics with Coupling to an External Bath. *J. Chem. Phys.* **1984**, *81*, 3684−3690.

(26) Lindahl, E.; Hess, B.; van der Spoel, D. Gromacs 3.0: A Package for Molecular Simulation and Trajectory Analysis. *J. Mol. Model.* **2001**, *7*, 306−317.

(27) Pon, F. R.; Sun, Q.; Faller, R. Detailed Molecular Modelling Study on the Local Dynamics in Polyisoprene−Polystyrene Blends. **2006**, manuscript in preparation.

(28) Allen, M. P.; Tildesley, D. J. *Computer Simulation of Liquids*; Oxford University Press Inc.: New York, 1987.

(29) Sayle, R. A.; Milnerwhite, E. J. RASMOL: Biomolecular Graphics for All. *Comput. Corner* **1995**, *20*, 374−376.

(30) Kremer, K.; Grest, G. S. Dynamics of Entangled Linear Polymer Melts: A Molecular-Dynamics Simulation. *J. Chem. Phys.* **1990**, *92*, 5057−5086.

(31) Faller, R.; Pütz, M.; Müller-Plathe, F. Orientation Correlations in Simplified Models of Polymer Melts. *Int. J. Mod. Phys. C* **1999**, *10*, 355−360.

CT600065V